Journal of Applied Fluid Mechanics, Vol. 18, No. 3, pp. 710-727, 2025.
Available online at www.jafmonline.net, ISSN 1735-3572, EISSN 1735-3645.
https://doi.org/10.47176/jafm.18.3.2871

Numerical Study of the Aerodynamic Effect of Ski Suit Surface Roughness on Ski Jumping Athletes During the Flight Phase

K. Liu[1,2,3], Z. Wang[2] and Q. Liu[1,2,3†]

[1] *State Key Laboratory of Mechanical Behavior and System Safety of Traffic Engineering Structures, Shijiazhuang Tiedao University, Shijiazhuang, 050043, China*
[2] *School of Civil Engineering, Shijiazhuang Tiedao University, Shijiazhuang, 050043, China*
[3] *Innovation Center for Wind Engineering and Wind Energy Technology of Hebei Province, Shijiazhuang, 050043, China*

†*Corresponding Author Email: qk@stdu.edu.cn*

ABSTRACT

Surface roughness of ski suits can have a significant effect on the aerodynamic performance of ski jumping athletes. Herein, several typical surface roughness configurations are examined through numerical simulations. Force parameters such as lift, drag and pitching moment are analyzed to evaluate the aerodynamic performance of varying surface roughness. Furthermore, the athlete model is segmented into distinct body parts to conduct a comprehensive analysis of the aerodynamic contributions from each individual segment. Generally, the surface roughness has a significant effect on the aerodynamic performance during the flight phase. Specifically, the lift–drag ratio of the entire multibody system shows a trend of increasing first and then decreasing. Moreover, the trunk of the athlete plays a predominant role in generating aerodynamic forces during the flight phase. Therefore, when designing high-performance ski jumping suits, prioritizing the surface roughness of this part can be considered first. Flow structures are also presented to analyze the impact of these various surface roughness conditions. Notably, flow suppression near the back region of the athlete body can significantly reduce the resistance force in the horizontal direction. Consequently, this revelation of the impact mechanism of ski suit surface roughness on the aerodynamic performance of the multibody system can guide the design of appropriate ski suits, and will also assist athletes in achieving superior aerodynamic performance during flight.

Article History

Received June 2, 2024
Revised August 27, 2024
Accepted October 1, 2024
Available online January 1, 2025

Keywords:

Ski-suits
Surface roughness
Aerodynamic performance
Numerical simulation

1. INTRODUCTION

In sports competitions, the performance differentials among elite athletes are frequently marginal, often residing within the purview of equipment and nuances in attire that can subtly affect outcomes (Liu et al., 2024). Hydrodynamic/aerodynamic performance plays an important role in racing sports, such as swimming, running, cycling, downhill skiing, luge, speed skating, sprinting, and, especially, ski jumping (Nazemi et al., 2018). Zhao and Ma (2021) noted that appropriate clothing materials can significantly enhance the overall level of competitive sports. Additionally, a previous study (Laing & Sleivert, 2002) has shown that appropriate clothing materials can reduce drag for athletes by up to 10%. Therefore, the hydrodynamic/aerodynamic features of clothing could play a pivotal role in helping athletes achieve optimal performance.

Appropriate fabrics are essential for improving athlete performance, and surface roughness is one of the key design parameters for clothing fabrics. Under the influence of wind, different roughnesses of clothing fabrics have different effects on aerodynamic features, which can directly affect the lift and drag forces acting on an athlete. The impact of the surface roughness of ski suits on aerodynamic performance has been studied in many ice and snow events. In early wind tunnel studies (Oggiano et al., 2009; Oggiano et al., 2012) on the surface roughness of ski suits for alpine skiing, athlete arms and legs were simplified as cylinders. The lift and drag coefficients of these cylinders with the same surface roughness as the ski suits were measured. Rough ski suits could reduce drag under certain conditions. Moreover, the effect of roughness on aerodynamic performance was studied by comparing the simplified cylinder model to the actual leg model. The results revealed that the conclusions of the two research methods are somewhat similar. Researchers

NOMENCLATURE

x	streamwise direction	U_0	freestream velocity
y	transverse direction	K_s	equivalent sand-grain roughness
z	spanwise direction	K_r	relative roughness
$\overline{C}_D$	mean drag coefficient	R_a	surface's geometric roughness height
$\overline{C}_L$	mean lift coefficient	Q	three-dimensional vortical scalar
$\overline{C}_p$	mean pressure coefficient	α	angle between the skis and the moving direction of the athlete (x direction)
$\overline{C}_f$	mean skin friction coefficient	β	upper body flexion angle
y^+	nondimensional wall-normal distance	θ	angle between the skis and the legs
$\overline{y^+}$	mean nondimensional wall-normal distance	φ	angle of attack
u_r	friction velocity at the wall	λ	angle between the two skis
U	local velocity	BMI	Body Mass Index

(Pugh, 1970) have also conducted wind tunnel experiments to verify that the transition from laminar to turbulent flow around athletes reduces surface resistance. The results showed that the study of the critical wind speed acting on an athlete's surface is closely related to the study of fluid flow over bluff bodies, especially spheres and cylinders. Moon et al. (2016) investigated the influence of different fabrics on the drag of speed skating athletes via a combination of numerical simulations and wind tunnel experiments. The experimental results were analyzed via particle image velocimetry (PIV), which provided an intuitive explanation of the mechanism by which new fabrics affect the aerodynamic performance of athletes.

Currently, there are many studies on the aerodynamic performance of ski jumping related to the athlete's posture, environmental wind, and ski equipment and their impact on the athlete's final results. However, few studies have investigated the impact of ski suit surface roughness on ski jumpers. Currently, methods for studying the flight phase of ski jumping include wind tunnel testing, field measurements, and numerical simulations. Schwameder et al. (2005) and Virmavirta et al. (2005) conducted field measurements to investigate the early flight phase. A larger forward lean could increase the flight distance to some extent, and entering the stable flight phase earlier may be beneficial to the athlete's overall performance. Additionally, Virmavirta et al. (Virmavirta et al., 2001; Virmavirta & Kivekäs, 2019) investigated the aerodynamic effect of skis on athlete performance. These studies revealed the variation patterns of the aerodynamic performance of the ski jump with changing wind angles of attack. Seo et al. (2004) conducted wind tunnel experiments to obtain the aerodynamic forces (lift, drag, and pitching moment) of a V-style ski jump and established an aerodynamic database for V-style ski jumping. Fritz et al. (2019) designed a more accurate force-measuring device that provides reliable support for better understanding the entire process of ski jumping. Elfmark et al. (2021) used field measurement methods to measure the flight speed and changes in lift and drag during the flight phase of ski jumping and analyzed the entire process of ski jumping comprehensively.

The abovementioned researchers have made some significant contributions to the study of the aerodynamic performance of ski jumping and have executed computational fluid dynamics (CFD) in their studies. However, most of these related studies have focused on the impact of the athlete's posture, skis, and wind conditions, and relatively little research has been conducted on the surface roughness of ski suits. The impact of this roughness of fabric cannot be neglected. This effect of the surface roughness of a ski suit is comprehensively studied via a numerical method. Moreover, each part of an athlete's body is investigated separately, which differs from previous studies that have focused on the whole body with a uniformly distributed surface roughness. The optimal surface roughness of each part is employed to generate better aerodynamic performance. Thus, this combination of surface roughness of ski suits can also provide more design possibilities for ski suits.

1.1. Contribution

The present study provides a comprehensive investigation into how the surface roughness of ski suits impacts the aerodynamic performance of ski jumpers during the flight phase by utilizing a high-fidelity numerical method. In general, this study analyzed the contribution of each part of an athlete's body to the total aerodynamic load. The proportions of lift and drag forces on various body parts of ski jumpers wearing ski suits with different surface roughnesses during flight were determined. Furthermore, this study explores the mechanism by which the surface roughness of ski suits impacts aerodynamic performance during the flight phase, which is elucidated through visual displays of the flow field around this system.

1.2. Paper Overview

In Section 2, the numerical methods and simulation setup are introduced. The verification and validation of the computational model are also presented in this section. In Section 3, the aerodynamic performance of the entire system with various surface roughnesses is investigated first. Both the force and the high-fidelity flow field are comprehensively analyzed. Next, the contribution of each

Table 1 Geometric dimensions of the athlete and the skis

Athlete's body			Skis		
Height (m)	BMI	Sitting height ratio (SHR)	Length (m)	Width (m)	Thickness (m)
1.77	19.5	0.532	2.58	0.115	0.01

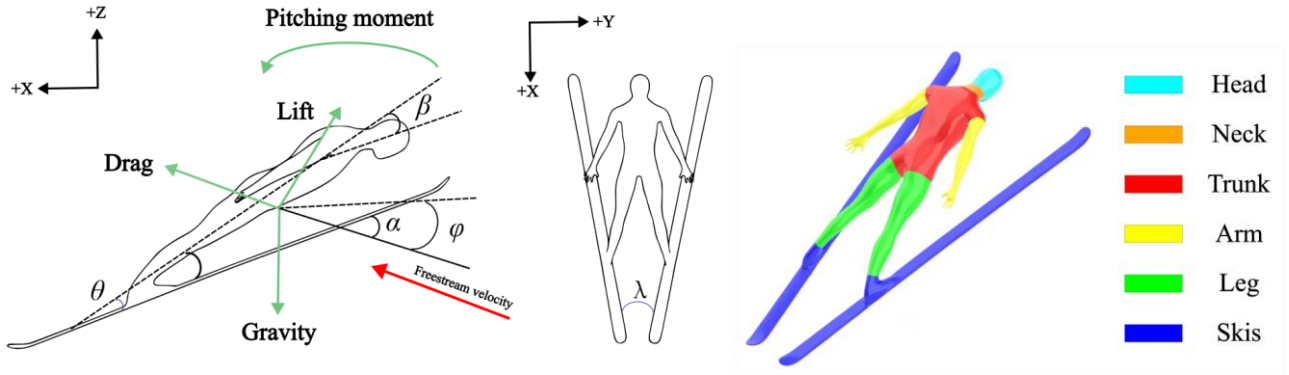

(a) (b)

Fig. 1 (a) Schematic diagram of posture parameters and force directions during flight; (b) different parts of the multibody system

part of the athlete's body to the overall aerodynamic performance is studied. Specifically, key parts such as the limbs and trunk and the surrounding flow are investigated individually to reveal the physics that leads to fluctuations in the forces. Eventually, the optimal design of surface roughness is discussed. Moreover, the rationality of this simplified model is examined. Section 4 concludes the study and discusses possible future work.

2. METHODOLOGY

2.1. Numerical Models

In this study, a 3-dimensional (3D) model of a ski jumping athlete that includes both the athlete's body and the skis is established. Specifically, the height and body mass index (BMI) of the athlete are generated according to the average values obtained via Müller's statistical analysis (Müller et al., 2006). The geometric dimensions of the athlete and the skis are presented in Table 1.

A schematic diagram of the posture parameters and force directions during flight is shown in Fig. 1. Note that this posture with various relative angles was established in previous studies (Seo et al., 2004; Ryu et al., 2015; Gardan et al., 2017). Specifically, there are five angles in Fig. 1, named $\alpha, \beta, \theta, \varphi$, and λ. Herein, α, which is 15°, is the angle between the skis and the moving direction of the athlete (x direction). β is the upper body flexion angle, which is 10°. The angle θ, which is 20°, represents the angle between the skis and the legs. φ is the angle of attack in this study and is 15°. The angle between the two skis, denoted λ, is 27.5°. In this research, the freestream velocity, which represents the relative velocity during the flight of the athlete, is fixed at 29 m/s according to field tests conducted by other researchers (Meile et al., 2006; Yamamoto et al., 2016).

In this study, the effects of surface roughness on different parts of an athlete's body are investigated. The entire system is divided into six parts: head, neck, trunk, arm, leg, and skis. These parts are marked with the different colors displayed in Fig. 1 (b).

In the numerical model, the surface roughness of the ski suit is controlled by varying the equivalent sand-grain roughness K_s and roughness constant C_s under the wall boundary conditions (Tauviqirrahman et al., 2021). K_s is used to represent the geometric height. When this value is set to 0, the wall is considered a smooth surface. This C_s is used to represent the degree of uneven distribution of the surface roughness, which is considered uniformly distributed when this value is set to 0.5. Notably, the equivalent sand-grain roughness K_s is not exactly the same as the surface's geometric roughness height, Ra. The specific differences are illustrated in Fig. 2. This study employs the conversion relationship derived from experiments by Adams et al. (2012). The specific conversion formula between K_s and Ra is $K_s = 5.863Ra$. To investigate the optimal design of the athlete's suit, typical geometric surface roughness heights from 0 μm to 81 μm are employed, which are from Chowdhury and Alam (2014) . Note that the skis have a smooth wall boundary, indicating that the surface roughness is 0 μm in all the simulations. In this study, only the surface roughness values of the arms, trunk and legs, which are covered by the ski suit, are modified.

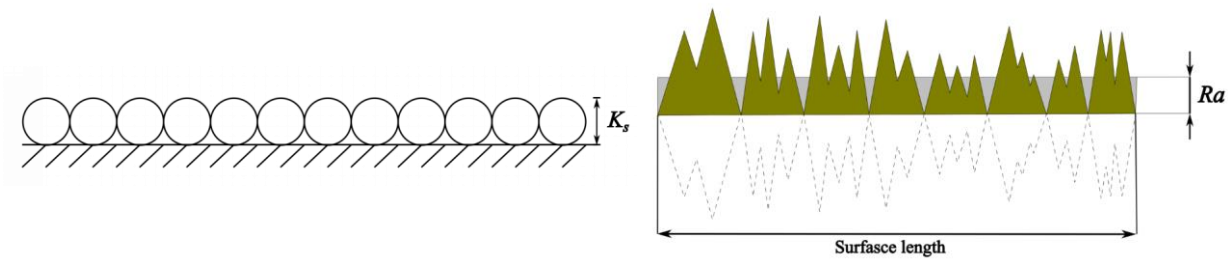

(a) (b)

Fig. 2 Illustration of surface roughness height and equivalent sand-grain height: (a) uniform sand-grain roughness model; (b) roughness profile

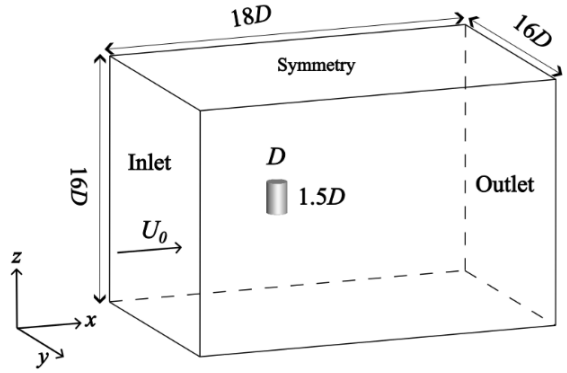

Fig. 3 Schematic diagram and boundary conditions of the finite cylinder model

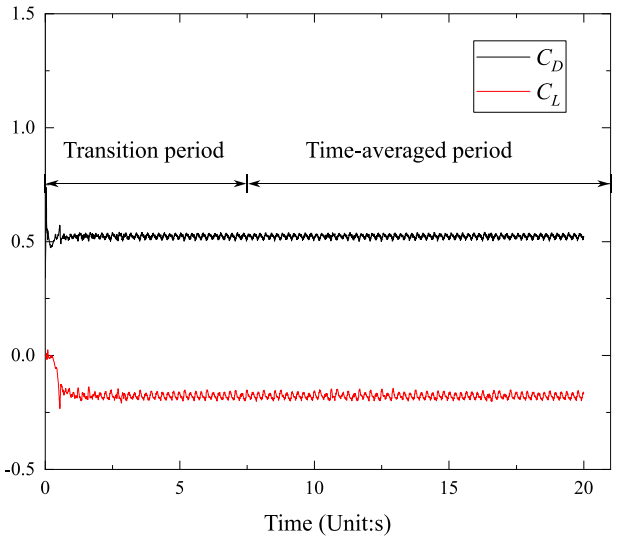

Fig. 4 Time-dependent lift and drag coefficients of the finite cylinder model

2.2. Verification and Validation

In this study, a model of a finite-length cylinder is initially established to demonstrate the accuracy and robustness of the numerical solver and setups. A timestep size-independent study is conducted via this model, with the results subsequently compared with those from previous studies. Four meshes with varying numbers of elements are subsequently generated for the athlete's body to conduct a mesh independence study. Finally, the study concludes by summarizing and comparing other relevant research that used ski jumping athlete models, directly comparing these findings to the results obtained in this study.

A schematic diagram and the boundary conditions of this finite cylinder model are presented in Fig. 3. The computational domain was configured with a velocity inlet at the inlet and a pressure outlet at the outlet. The top, bottom, front, and back surfaces of the domain were assigned symmetry boundary conditions, while the cylinder surface was set as a no-slip wall (Wang et al., 2024). The number of mesh elements for this model is approximately 3.0×10^6. All the numerical simulations are conducted via ANSYS® Fluent® 20.0 software. Note that both a shear stress transport (SST, k-ω) model and an SST−scale-adaptive simulation (SST−SAS) turbulence model are adopted for this verification and validation test.

At the initial stage, a time step size-independent study is carried out with the SST−SAS turbulence model at a Reynolds number of 2.5×10^5. Within three different time step sizes (0.04 s, 0.004 s and 0.001 s), there is a marginal difference between the results obtained by dt=0.004 s and those obtained by dt=0.001 s. Therefore, the time-step size dt=0.004 s is selected for the finite cylinder model. Concurrently, the initial 7.5 seconds were assigned as the transition phase, while the period from 12.5 to 20 seconds was allocated as the time-averaged segment, as illustrated in Fig. 4.

Next, the results of the finite-length cylinder with various Reynolds numbers are compared with those of previous numerical studies (Gao et al., 2018; Prosser & Smith, 2016; Chowdhury & Alam, 2014; Zdravkovich et al. 1989), the results of which are presented in Fig. 5, where K_r is the relative roughness defined as K_s/D. This figure shows that the $\overline{C}_D$ values obtained by both the SST k-ω and the SST−SAS turbulence models are in good agreement with previous research. Additionally, the SST−SAS model has been validated to be reliable in many aerodynamic applications (Gao et al., 2018; Wang et al., 2024), making it adequate for investigating unsteady flow around an athlete.

A grid independence study is conducted by employing the athlete model shown in Fig. 6 (a). The boundary condition setups and the geometric dimensions

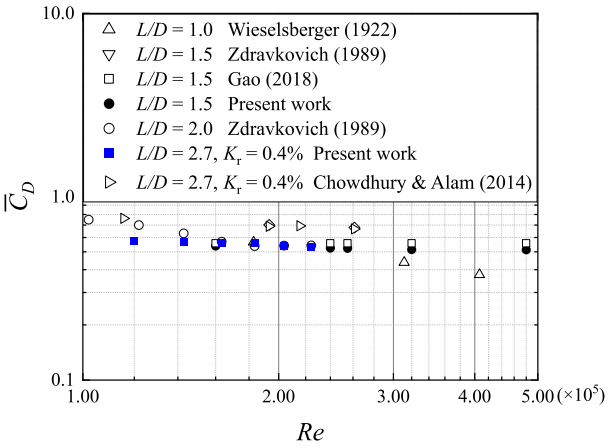

Fig. 5 $\overline{C}_D$ obtained with different Reynolds numbers and turbulence models for a cylinder of finite length

of the computational domain are shown in Fig. 6(a). The computational domain was set up with a velocity inlet at the entrance and a pressure outlet at the exit. Symmetry boundary conditions were applied to the top, bottom, front, and back surfaces of the domain, while the entire surface of the system was configured as a no-slip wall. In this study, a hexahedral mesh is adopted, as displayed in Fig. 6 (b). A refinement zone exists near the athlete's body and the wake region, which is also shown in Fig. 6 (b), to generate high-fidelity numerical simulations. Additionally, inflation layers are adopted around the athlete's body to precisely capture the small flow features. The Reynolds number for this test, which is calculated on the basis of previous research (Yamamoto et al., 2016), is 3.51×10^6. Four different meshes, which have 10.18 million, 12.70 million, 16.39 million, and 20.36 million elements, are tested. Note that the mean y^+ values of all the cases near the athlete's body are approximately 1. The results of the ratio of the lift force to drag force are compared. The ratios obtained by different meshes are almost identical and are approximately 1.85. Therefore, to reduce the computational cost, a mesh with 10.18 million elements is selected for all the simulations in the remainder of this paper. Considering the intricate geometric structure of the athlete model, a time step of 0.001 s was selected. As depicted in Fig. 7, the initial second is allocated as the transition period, whereas the second and third seconds are assigned as the time-averaged period.

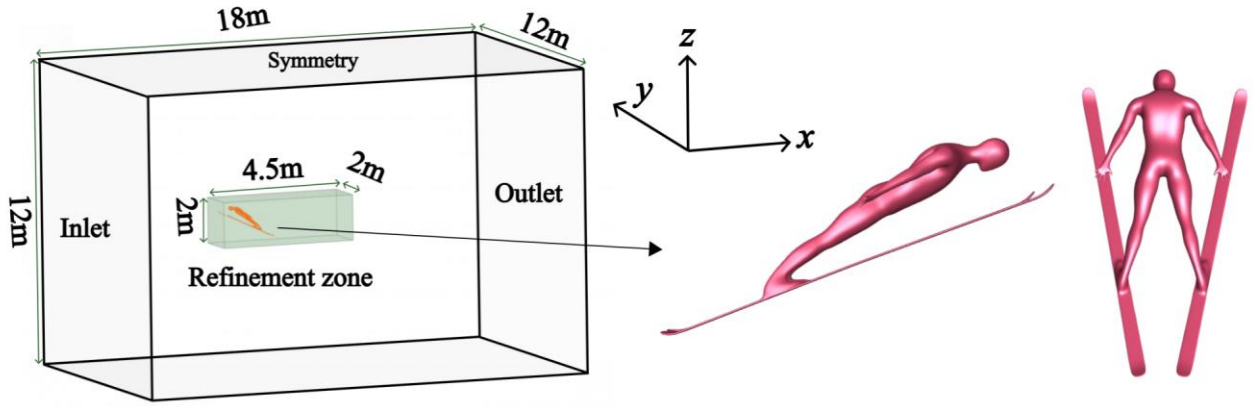

(a)

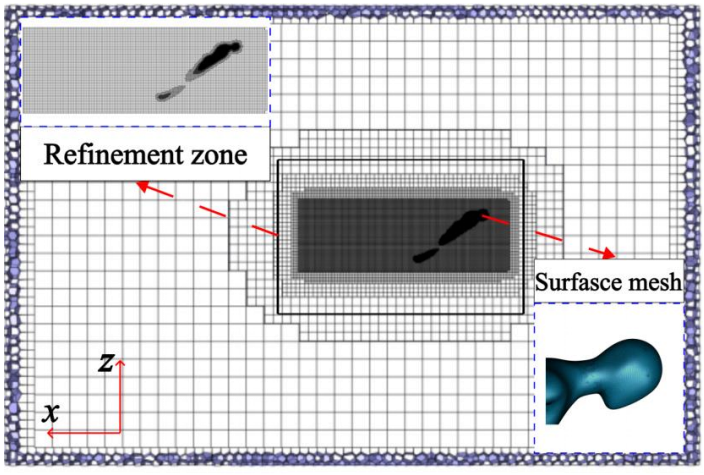

(b)

Fig. 6 (a) Boundary conditions and geometric dimensions of the computational domain; (b) grid setup

Table 2 Model validation and comparative results for the ski jumping athlete

Method	Velocity	φ	λ	θ	Lift–drag ratio
Numerical simulation (k-ω model) (Gardan et al., 2017)	29.0 m/s	29°	38°	17°	1.91
Wind tunnel experiment (Chowdhury et al., 2011)	27.8 m/s	10°	30°	30°	1.48
	30.6 m/s	10°	30°	30°	1.53
On-site measurement (Elfmark et al., 2021)	27.8 m/s	—	—	—	1.47
	30.6 m/s	—	—	—	1.53
Current work (SST–SAS model)	29.0 m/s	25°	28°	25°	1.48

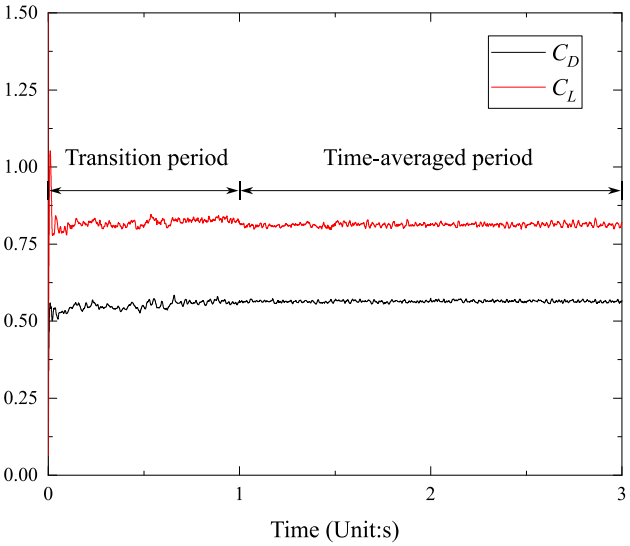

Fig. 7 Time-dependent lift and drag coefficients of the ski-jumping athlete model

A typical case with a smooth surface is selected for comparison with previous research and is presented in Table 2. Table 2 shows that the lift–drag ratios in the current study are in good agreement with those obtained previously. The small variation could be attributed to the subtle difference in the geometric model and Reynolds number. The lift–drag ratio obtained by the current method is very similar to the findings of Chowdhury et al. (2011) and Elfmark et al. (2021), demonstrating that the numerical method is sufficient to resolve the flow problem around the multibody system of ski jumping athletes and skis.

3. RESULTS AND DISCUSSIONS

3.1. Study of the Aerodynamic Performance of Systems with Various Surface Roughnesses

3.1.1. Lift and Drag

The aerodynamic loads acting on the multibody system, which includes the athlete and skis, consist of lift and drag. The aerodynamic characteristics of the system, including the lift, drag and lift–drag ratios, are presented in Fig. 8 as a function of surface roughness. The impacts of the surface roughness height *Ra* on the whole system and the athlete are relatively similar. Specifically, when *Ra* is less than 28 μm, an increase in surface roughness leads to a progressive rise in the fluctuation of the lift-to-drag ratio for both the entire multi-body system and for the athlete and ski individually. Simultaneously, Fig. 8 illustrates that the lift and drag contributions of the human body constitute only approximately half of the total system, while the ski accounts for more than half. This observation effectively corroborates the significance of the aerodynamic performance of skis in the V-style skiing posture. (Virmavirta & Kivekäs, 2019; Cao et al., 2022; Zhang et al., 2022). Concurrently, there is a decrease in the individual drag and lift values when *Ra* increases from 0 μm to 28 μm. Beyond the 28 μm threshold, both the system and athlete experience a decrease in their lift–drag ratios. Notably, the lift–drag ratio of the entire system decreases from 1.49 to 1.44, whereas the athlete's ratio decreases from 1.28 to 1.20.

As *Ra* increases from 28 μm to 80 μm, the drag of the system and the athlete generally increases, where the maximum value occurs when *Ra* = 71 μm. In particular, the drag of the system increases from 153.79 N to 159.85 N. Meanwhile, the drag of the athlete increases from 77.74 N to 83.38 N. On the other hand, beyond this *Ra* threshold, the lift of both the entire system and the athlete remains relatively constant. Thus, the decrease in the lift–drag ratio within this range of *Ra* is due primarily to the increase in drag.

3.1.2. Pitching Moment

The combined force of lift and drag typically does not act at the center of mass of the multibody system, resulting in the generation of a moment. Herein, the moment about the y-axis with respect to the center of mass of the system is defined as the pitching moment. This pitching moment has a negative effect on the balance of the athlete during the flight phase. Therefore, this pitching moment is not negligible.

The pitching moments are measured with the center of mass of the system, which is composed of the athlete and skis, as the center of rotation. A positive pitching moment indicates that the combined effect of lift and drag causes the athlete to lean backward, whereas a negative value signifies a moment that causes the athlete to lean forward. Fig. 9 presents the pitching moment of the system and the athlete with different surface geometric roughness heights *Ra*. The impact of surface roughness on the pitching moment is relatively slight. Furthermore, the positive aerodynamic pitching moment acting on the athlete indicates a tendency to lean forward, whereas the negative pitching moment acting on the skis indicates a tendency to lean backward. The total aerodynamic pitching

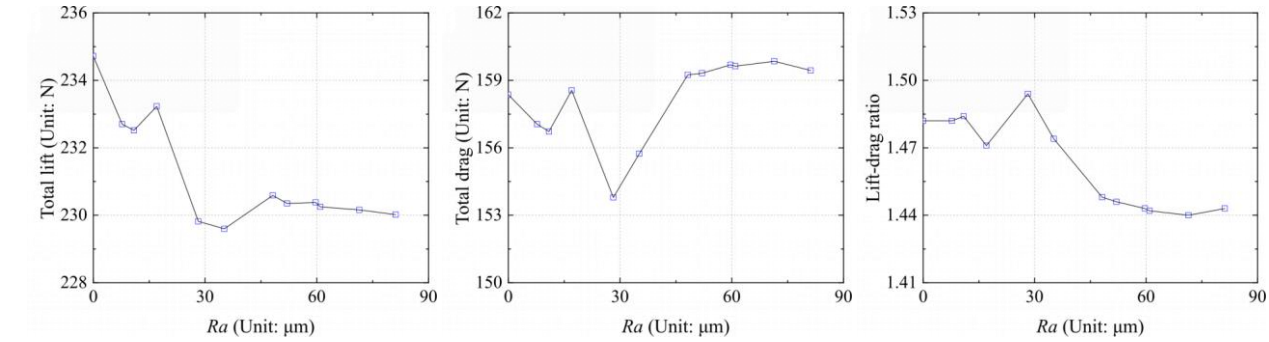

(a) Entire system

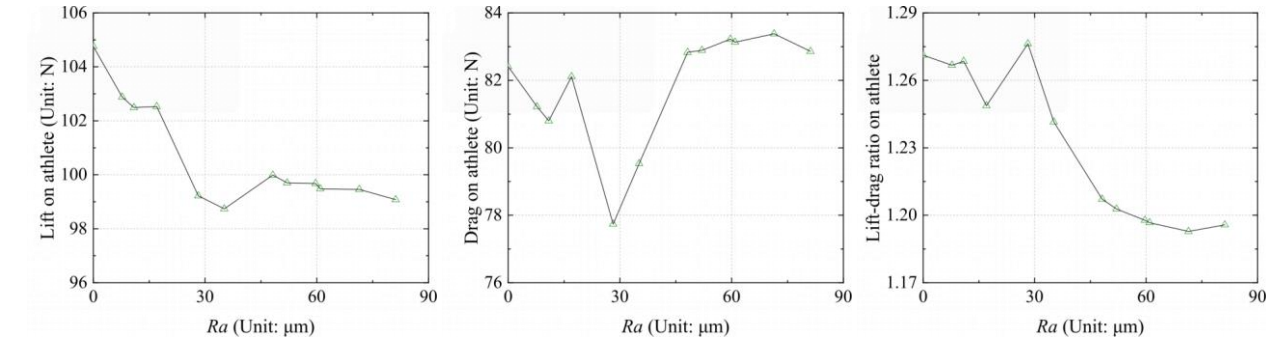

(b) Athlete

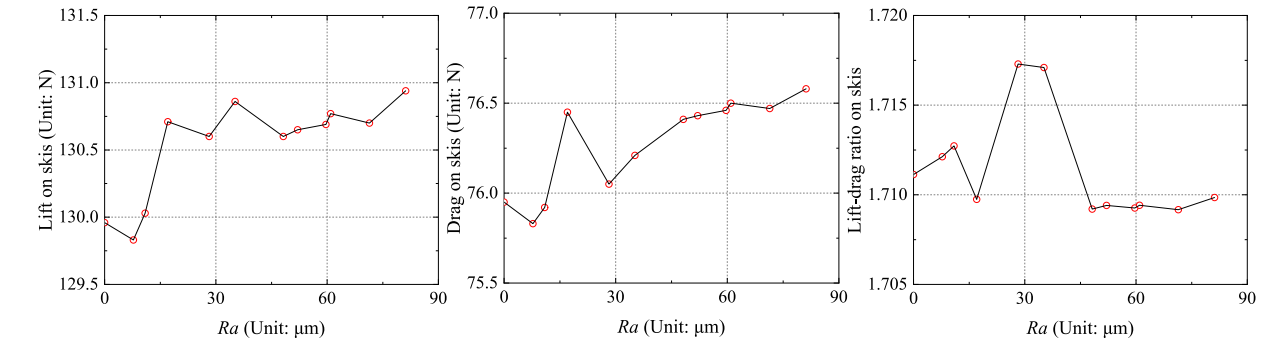

(c) Skis

Fig. 8 Aerodynamic characteristics of the systems as a function of surface roughness: (a) entire system; (b) athlete; (c)skis

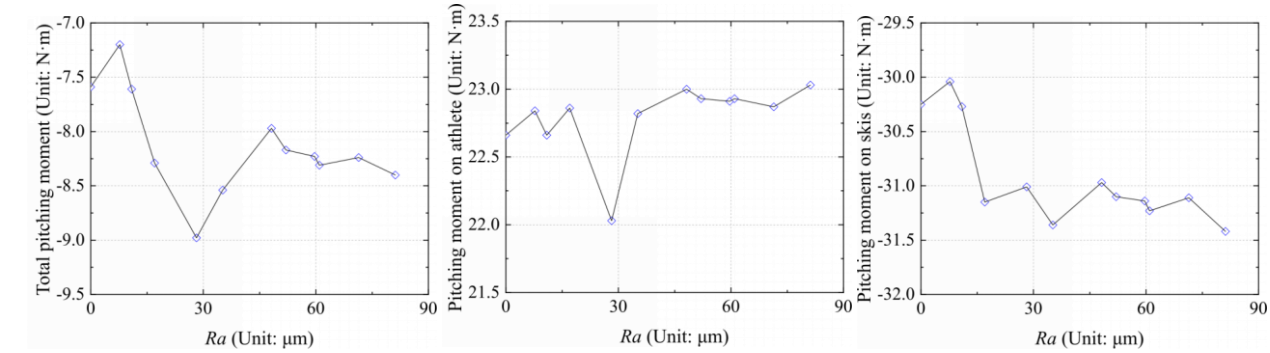

(a) (b) (c)

Fig. 9 Pitching moment of (a) the entire system; (b) the athlete; and (c) skis

moment of the system is a moderate negative value because of the combination of the moments acting on the athlete and the skis. This pitching moment reaches its maximum absolute value when *Ra* is 28 μm, which simultaneously results in the highest lift–drag ratio. Thus, the surface roughness of 28 μm leading to the highest lift–drag ratio results in the most unfavorable ability to maintain stability during athlete flight. The geometric surface roughness height *Ra* of 8 μm has the lowest pitching moment and a relatively high lift–drag ratio (1.48), which is close to that obtained for a surface roughness of 28 μm (1.49). Therefore, the 8 μm surface roughness is selected as the optimal value in this study.

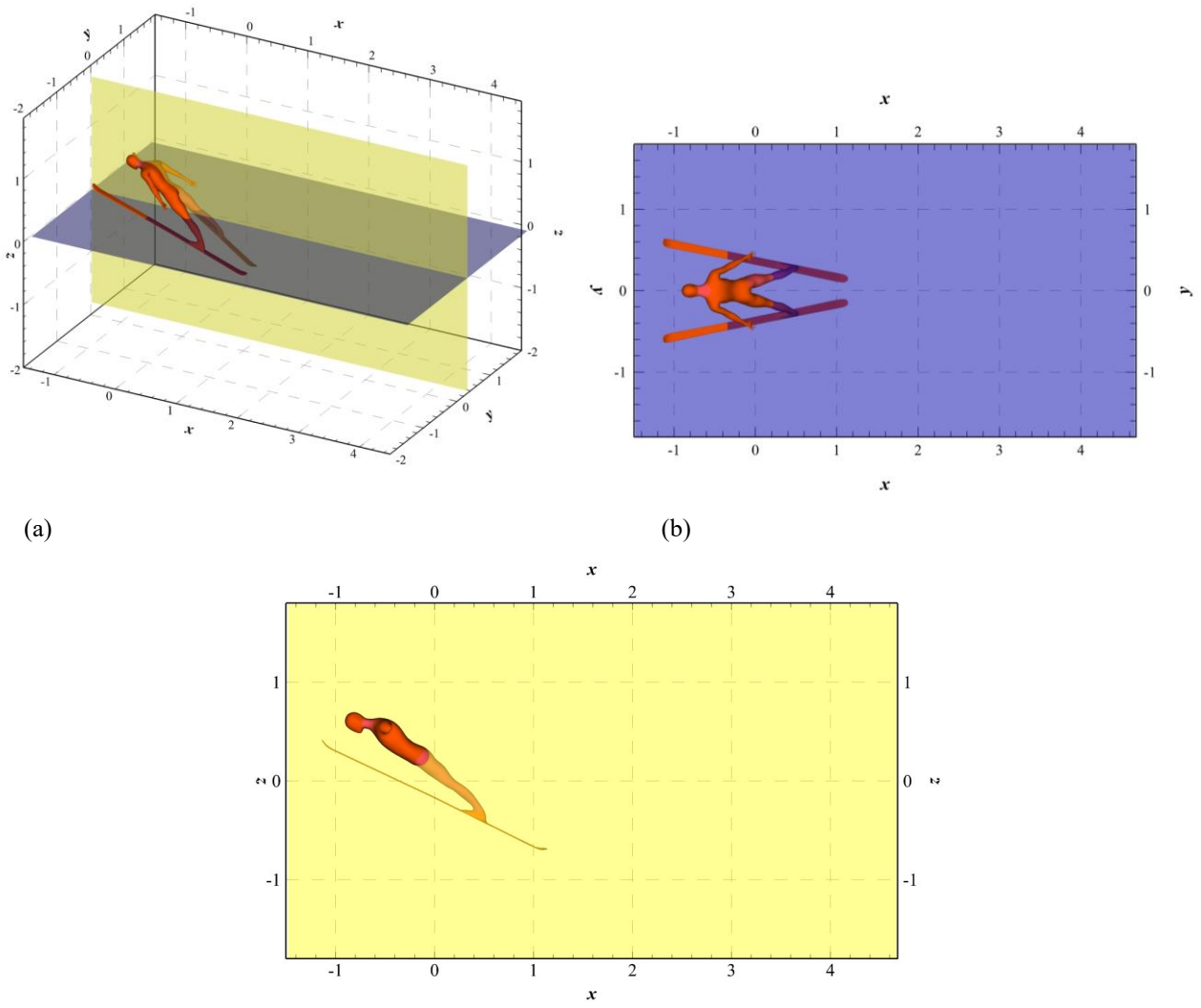

Fig. 10 Schematic diagrams showing the (a) elevation view; (b) *z* = 0 plane; and (c) *y* = 0 plane

3.1.3. Flow Field Analysis

The analysis of pressure and streamline distributions around an athlete is particularly important for understanding the impact mechanism of surface roughness on ski suits. Therefore, two mutually perpendicular planes passing through the center of mass of the multibody system comprising the athlete and skis are selected for studying the flow field morphology around them. Specifically, the selected planes are at $y = 0$ and $z = 0$, with the schematic diagram of these planes shown in Fig. 10.

Figure 11presents the mean pressure contour and mean velocity streamline on the $y = 0$ plane (the direction of the velocity streamline is from left to right). The average pressure contours and velocity streamlines around the system exhibit highly similar characteristics at different roughness values. There is a distinct positive pressure region at the front of the head and chest, whereas there is a clear negative pressure region above the back and behind the buttocks. Moreover, a small recirculation vortex appears under the jaw, and the velocity streamlines from the back and front of the chest converge toward the buttocks.

Notably, the mean pressure contours and velocity streamlines around this system for surface roughness values of Ra = 28 μm and Ra = 35 μm are significantly different from those for other roughness values. As observed in Fig. 11, under these two roughness conditions, the streamlines behind the athlete's buttocks are straighter and form a larger angle with the horizontal direction. Moreover, the negative pressure area behind the multibody system is significantly reduced compared with that under other conditions. These two flow field conditions, which are significantly different from the other flow field conditions, are consistent with the conditions that result in the least drag, as analyzed from Fig. 8 (b).

Similarly, from Fig. 12 on the $z = 0$ plane, the mean pressure contour and mean velocity streamlines also show significant differences for Ra = 28 μm and Ra = 35 μm compared with those for other Ra values. In Fig. 12, under these two roughness conditions, the streamlines behind the system are more symmetric, and a radial streamline

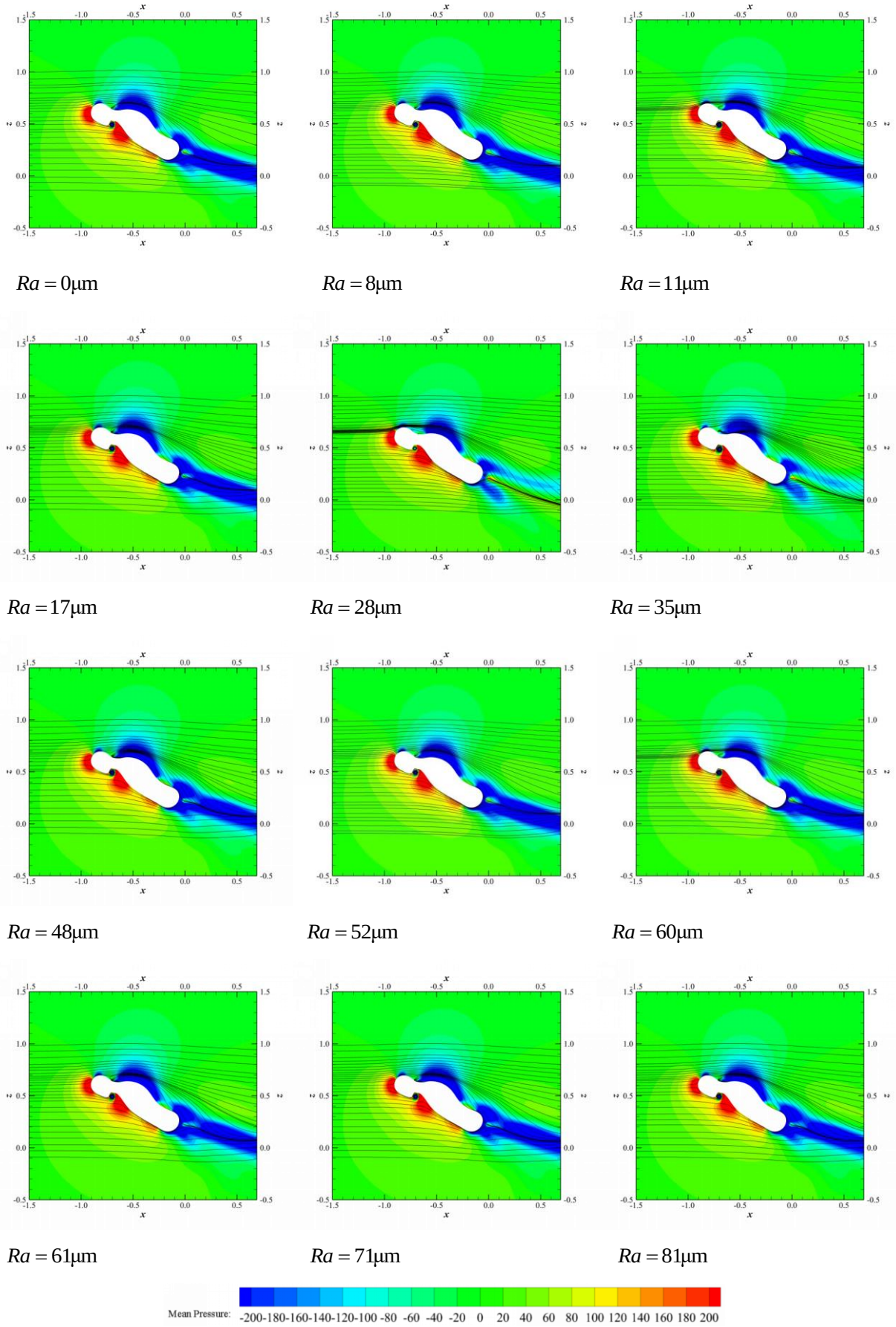

Fig. 11 Pressure distribution and streamlines on the *y* = 0 plane with different *Ra* values

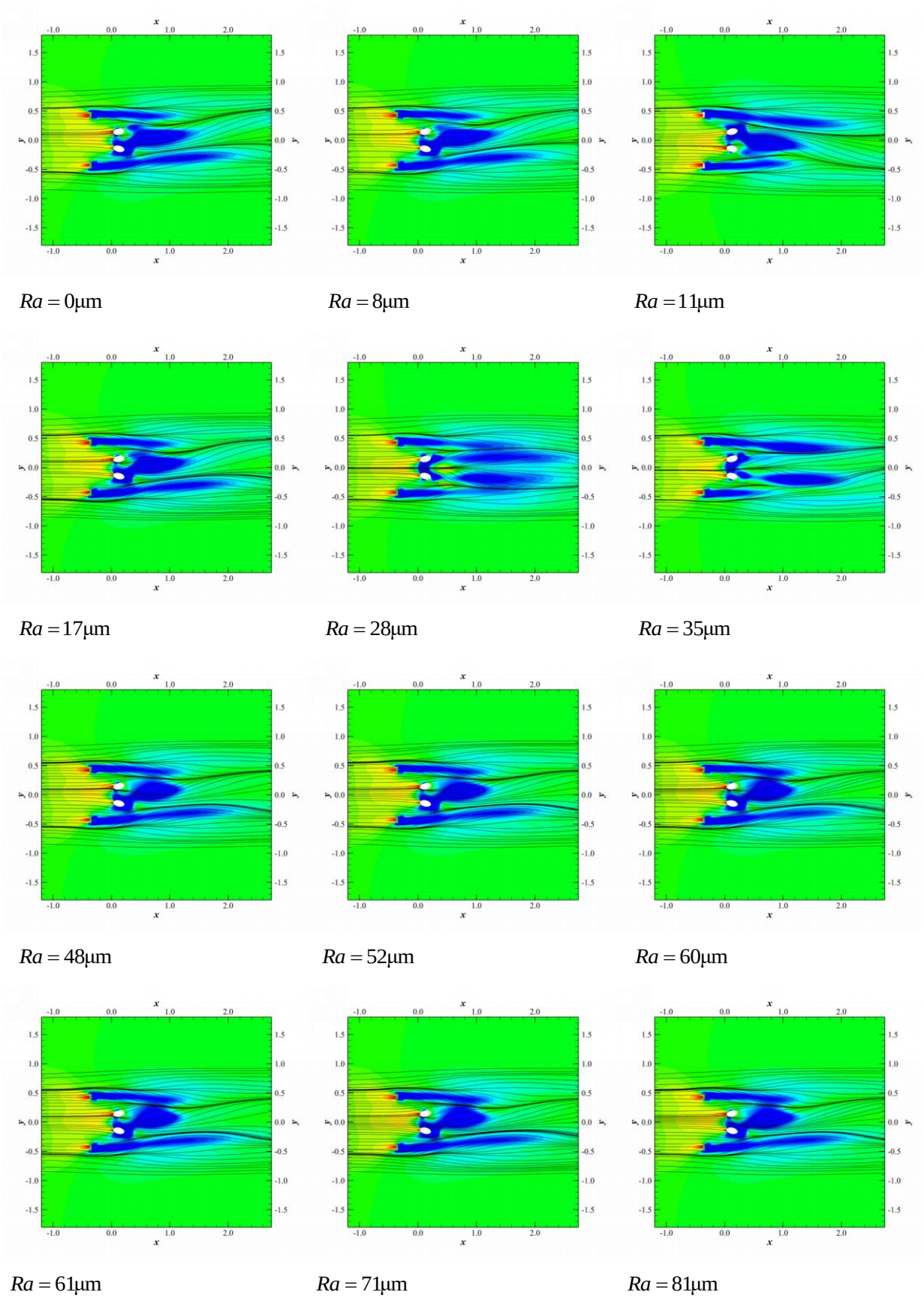

Fig. 12 Pressure distribution and streamlines on the *z* = 0 plane with different *Ra* values

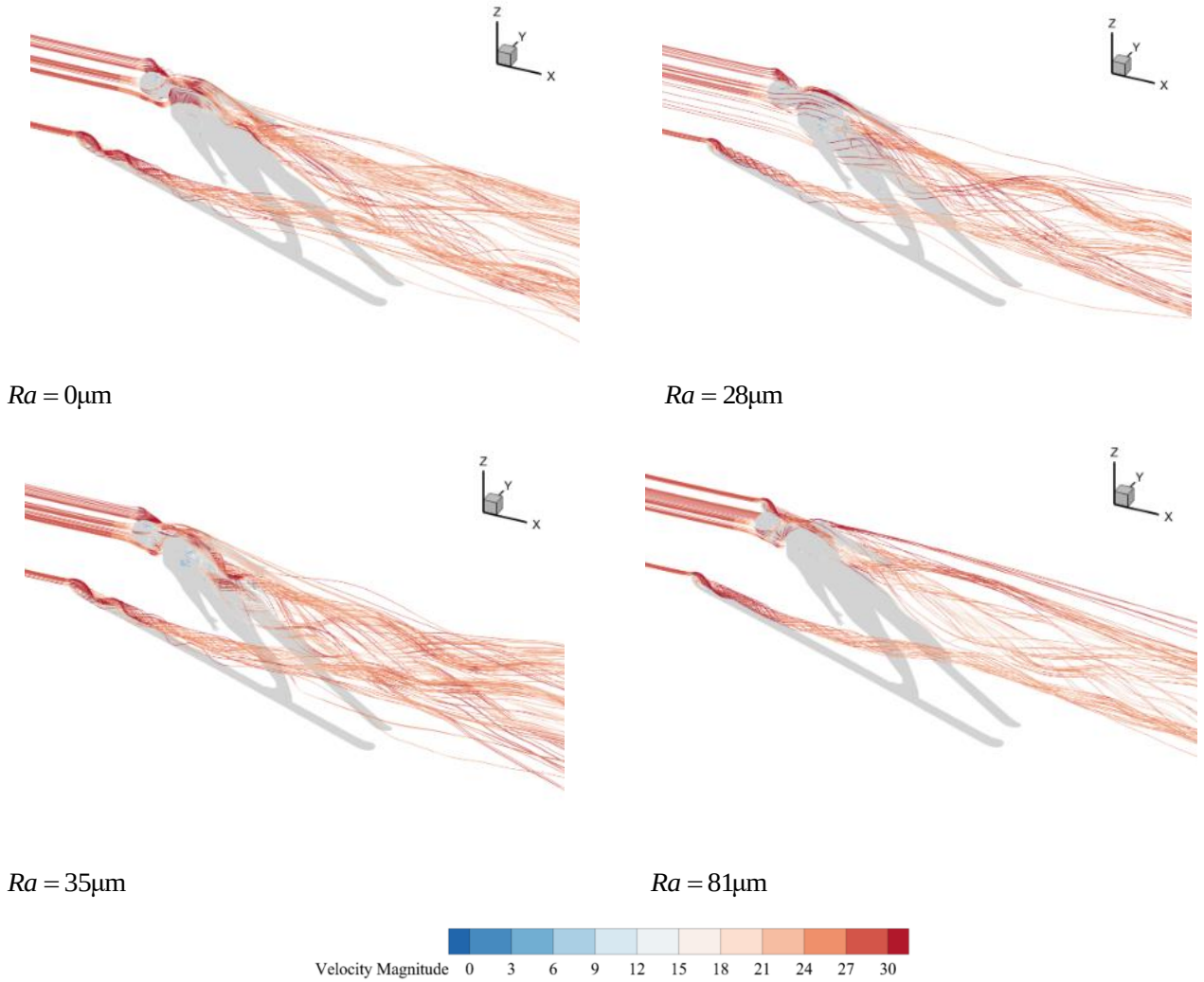

Fig. 13 Streamline patterns colored by instantaneous speed for a given speed of 29 m/s with different *Ra*

pattern diverging to both sides is evident behind the athlete's legs. Furthermore, the pressure distribution is significantly different under these conditions; the negative pressure area behind the system and near the surface of the legs separates more distinctly, moving farther from the body, which is more conducive to reducing the drag coefficient.

A careful observation of the three-dimensional streamline patterns, as shown in Fig. 13, reveals that with *Ra* = 28 μm and *Ra* = 35 μm, the flow in the wake of the athlete is closer to the athlete. However, when the roughness increases to 81 μm, the attachment of the flow behind the athlete significantly decreases. Comparison with Fig. 11 demonstrates that the distribution of the attachment region behind the athlete is intricately linked to the pressure coefficient distribution. Surface roughness can significantly impact flow separation behind the athlete, thereby affecting the pressure distribution.

Figure 14 shows the flow structures represented by iso-surfaces of the Q criterion with $Q = 40U_0^2/L^2$ marked by U/U_0 for different surface roughness conditions(Sohankar, 2014). Generally, it can be seen that those structures are similar with different surface roughness. The air flow firstly touches the ski and the head region. And then it separates around the head, neck and trunk. It can be observed that flow behind the trunk and ski has large separation to due to their geometric features. Thus, the ski and trunk contribute the major aerodynamic force. Meanwhile, rough surface can supress the flow separation behind the head. The flow structures behind the back change from vortex-like shape close to the back to linear shape state as it moves away from the back. From the Fig. 14, it also can be seen that there is a pronounced vortical structure in front of the chest, which becomes more asymmetric when the surface roughness increases. The U/U_0 distributions also show that there are relatively large velocity magnitude on the top of the head and the chest of the trunk. However, the large flow separation behind the head results in a "dynamic stall" effect that reduces the drag generated by the velocity magnitude on the head.

3.2. Study of the Aerodynamic Performance of the Arm/Trunk/Leg Sections

To further explore the mechanism by which the surface roughness impacts the mechanical performance of each part of the system, an analysis is conducted on the aerodynamic performance of the arms, trunk, and

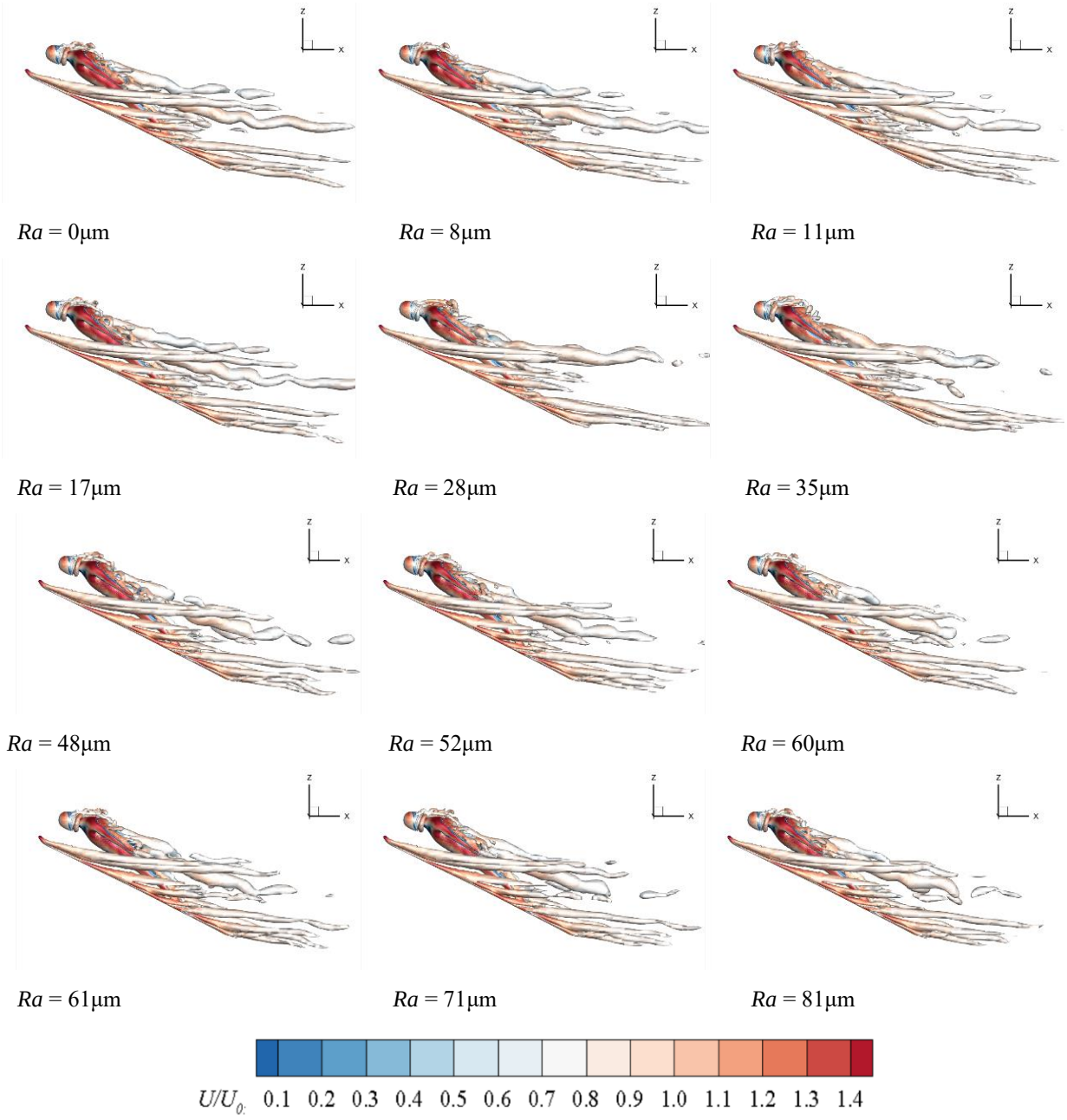

Fig. 14 Side of vortical structures represented by the iso-surface marked with U/U_0 of the Q criterion with $Q = 40U_0^2 / L^2$ with different *Ra*

legs. The drag experienced by each part during flight is divided into pressure drag and friction drag, and the factors influencing drag are complex. With similar trends, a smaller minimum pressure coefficient implies greater pressure drag, and a larger maximum surface friction coefficient indicates increased friction drag. Additionally, early flow separation can also increase drag. For ease of calculation and analysis, the lift and drag coefficients for the arms, trunk, and legs are computed via the frontal area of the entire system. Moreover, the flow separation is quantitatively described via the separation angle γ, which is defined by the typical flow separation around a cylinder, as illustrated in Fig. 15.

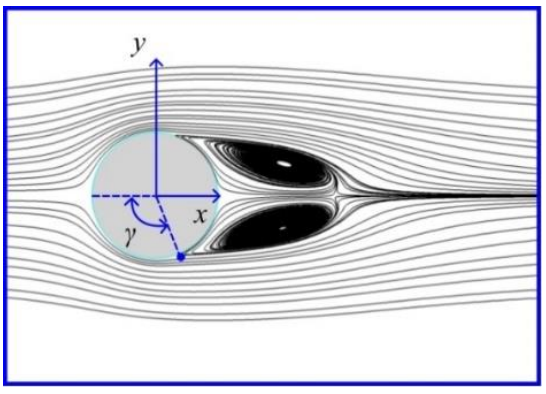

Fig. 15 Illustration of the separation angle

Table 3 Proportion of lift and drag for each part

	Head	Neck	Arms	Trunk	Legs	Skis
Lift	2.9%	4.4%	9.6%	21.4%	5.1%	56.6%
Drag	1.1%	2.6%	10.0%	24.7%	13.4%	48.2%

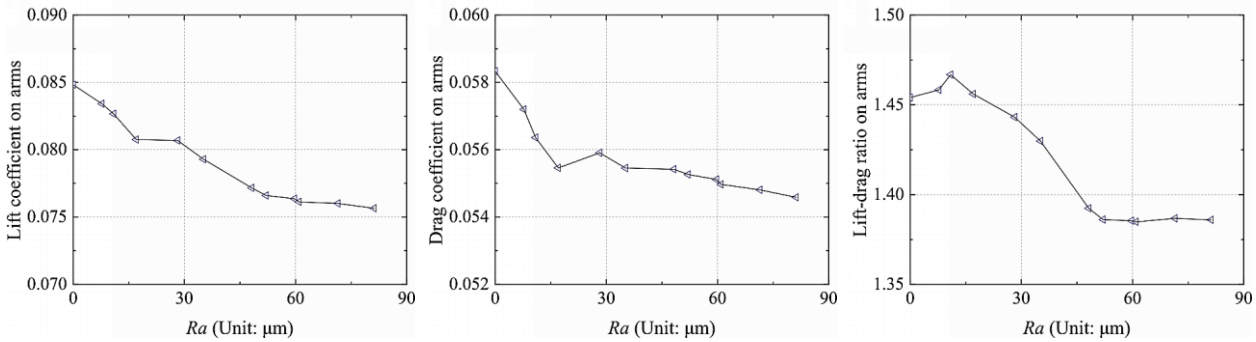

(a) (b) (c)

Fig. 16 Aerodynamic performance of the arms: (a) lift; (b) drag; and (c) lift–drag ratio

3.2.1. Proportion of Lift and Drag for Each Part

The proportions of lift and drag for each part are shown in Table 3. The trunk contributes to most of the lift and drag within the parts covered by the ski suits. The contribution by the limbs follows. Therefore, it is necessary to further study the aerodynamic mechanism of these parts.

3.2.2. Aerodynamic Performance of Arms

The aerodynamic performance of the arms is presented in Fig. 16. The figure shows that the lift, drag and lift−drag ratio generally decrease when the surface roughness increases, with occasional increases at certain points.

To further study the underlying mechanism, the time-averaged pressure coefficient $\overline{C_p}$ and time-averaged skin friction coefficient $\overline{C_f}$ at the middle position in the z-direction of the arm as a function of the circumferential angle are presented in Fig. 17. The pressure coefficient curves along the circumferential angle for the arm with different surface roughnesses almost overlap, indicating that surface roughness has a minor effect on the pressure drag of the arm. In Fig. 17 (b), for $Ra < 35$ μm, the surface friction coefficient of the arm increases with surface roughness, and the separation point gradually moves backward, remaining almost constant for $Ra > 35$ μm. Additionally, the smaller surface area of the arm leads to less friction drag. Therefore, when $Ra < 35$ μm, the continuous backward movement of the separation point causes a consistent decrease in the drag coefficient; when $Ra > 35$ μm, the position of the separation point remains nearly unchanged, and the drag coefficient stabilizes. This further explains the trend observed in Fig. 16, where the drag coefficient of the arm changes with increasing surface roughness. Consequently, the impact of surface roughness on the pressure drag of the arm and the position of the separation point is extremely small, as its influence on the drag coefficient is reflected primarily in the movement of the separation point; the backward movement of the separation point results in a decrease in the drag coefficient of the arm.

3.2.3. Aerodynamic Performance of the Trunk

Compared with the arm, the trunk possesses a more irregular geometric shape, and the impact of surface roughness on the trunk is more complex. The specific aerodynamic performance curves of the trunk with varying surface roughnesses are shown in Fig. 18. Additionally, curves depicting the circumferential distributions of the pressure coefficients and surface friction coefficients of the trunk for different surface roughnesses are presented in Fig. 19. By comparing Fig. 18 (b) (c) with Fig. 8 (b), the drag and lift−drag ratio experienced by the athlete and the trunk follow a very similar trend with increasing surface roughness. This similarity further reflects the significant impact of the trunk performance on the athlete's overall aerodynamic performance. Additionally, the lift coefficient of the trunk tends to fluctuate, with minimal changes in the lift coefficient as the surface roughness exceeds 35 μm. Additionally, Fig. 19 (a) shows that for most surface roughness values, the circumferential pressure coefficient curves of the trunk almost overlap, with only the conditions with $Ra = 17$ μm, 28 μm, and 35 μm showing significantly different pressure coefficient curves. Similarly, the friction coefficient curves in Fig. 19 (b) for $Ra = 0$ μm, 8 μm, 17 μm, and 35 μm also exhibit notable differences from the others. These trajectories of the pressure and surface friction coefficients in Fig. 19 effectively explain the trend of the drag coefficient in Fig. 18 (b).

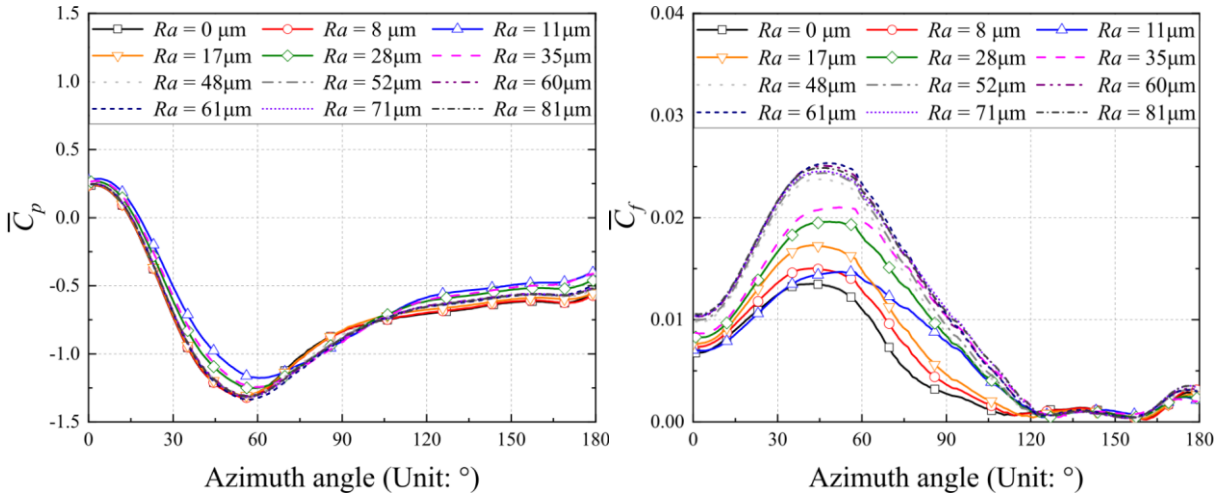

(a) (b)

Fig. 17 (a) Time-averaged pressure coefficient $\overline{C}_p$ and (b) time-averaged skin friction coefficient $\overline{C}_f$ at the middle position in the z-direction of the arm as a function of the circumferential angle

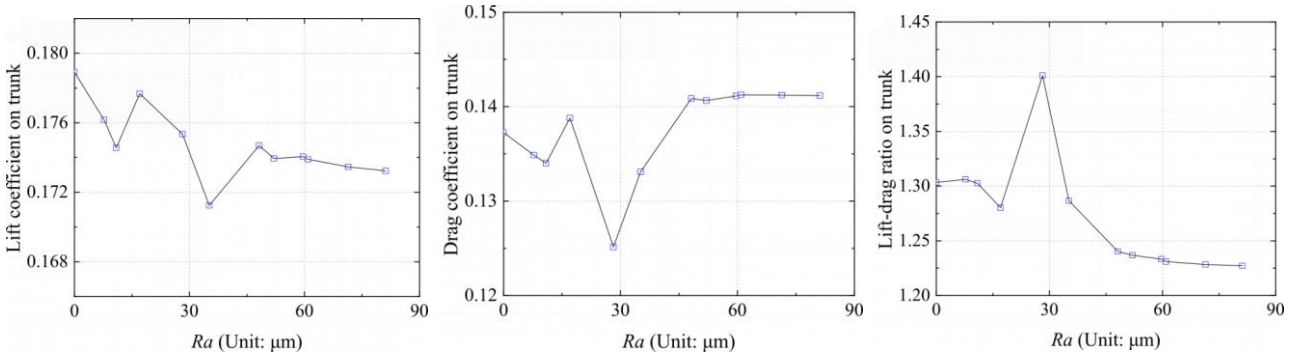

(a) (b) (c)

Fig. 18 Aerodynamic performance of the trunk: (a) lift; (b) drag; and (c) lift–drag ratio

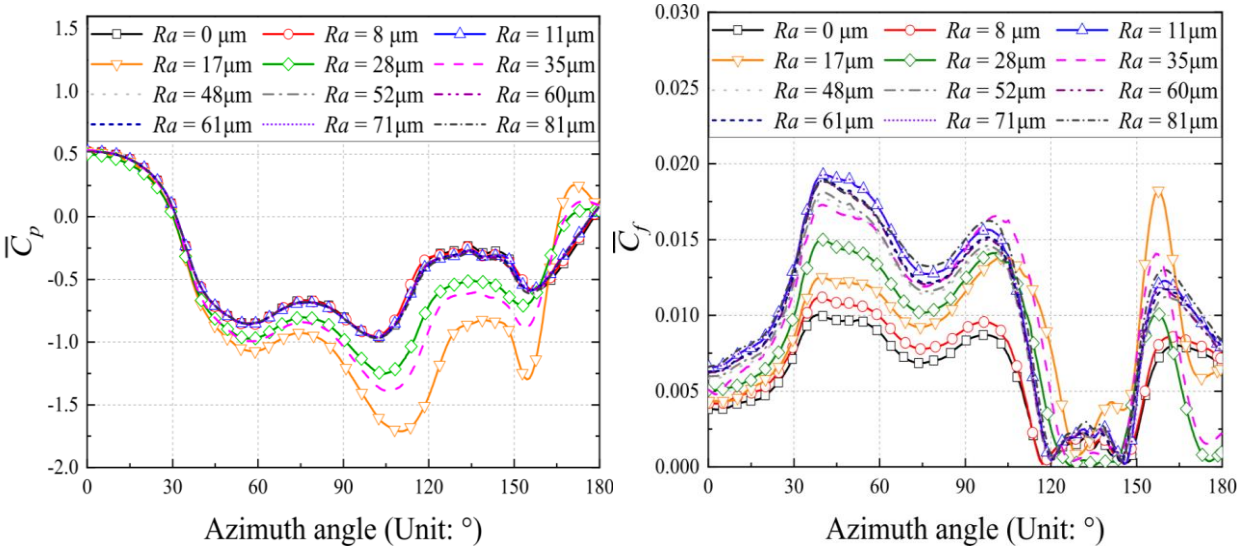

(a) (b)

Fig. 19 (a) Time-averaged pressure coefficient $\overline{C}_p$ and (b) time-averaged skin friction coefficient $\overline{C}_f$ at the middle position in the z direction of the trunk as a function of the circumferential angle

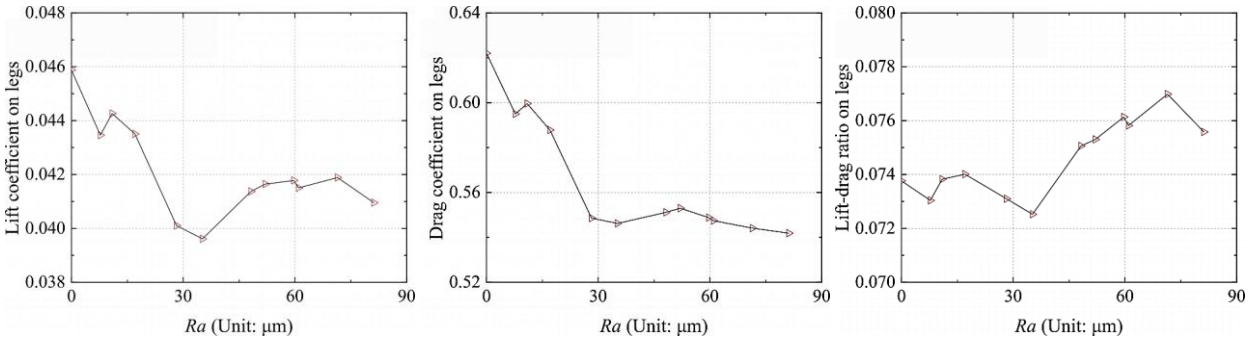

(a) (b) (c)

Fig. 20 Aerodynamic performance of the trunk: (a) lift; (b) drag; and (c) lift–drag ratio

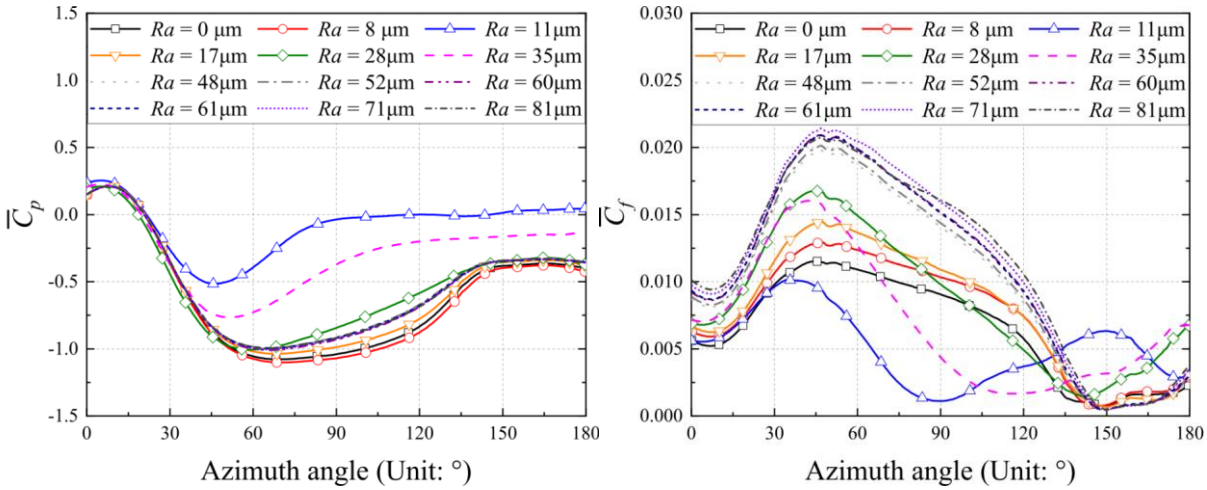

(a) (b)

Fig. 21 (a) Time-averaged pressure coefficient $\overline{C}_p$ and (b) time-averaged skin friction coefficient $\overline{C}_f$ at the middle position in the z direction of the legs as a function of the circumferential angle

When *Ra* < 17 μm, the drag coefficient decreases due to nearly constant pressure coefficients and increasing peak values of friction coefficients, whereas the separation angle shifts from 115.6° to 118.6°, a backward shift of 3.0°. This backward shift in separation angle plays a dominant role in reducing drag on the trunk. At *Ra* = 17 μm, a significant increase in pressure drag predominates over the increase in drag coefficient. When 17 μm < *Ra* < 52 μm, the pressure drag at surface roughnesses of 28 μm and 35 μm, despite having smaller minimum values of pressure coefficients, is accompanied by a forward shift in the separation angle from 123.2° to 118.5°, which is a shift of 4.7°. Therefore, the increasing maximum values of the surface friction coefficients, the forward shift in the separation angle and the increase in the maximum friction coefficients all lead to an increase in the drag coefficient.

When *Ra* exceeds 35 μm, the pressure coefficient and friction coefficient trajectories for different surface roughnesses tend to converge, which explains the nearly stable aerodynamic performance of the trunk within this roughness range.

3.2.4. Aerodynamic Performance of Legs

The variation in the mechanical performance of the legs with surface roughness is shown in Fig. 20. In the range of 0 μm < *Ra* < 35 μm, the drag first increases but then decreases. Fig. 21 shows that at *Ra* = 11 μm, the lowest pressure drag is observed, accompanied by the earliest flow separation. At *Ra* = 35 μm, a similar low-pressure drag is noted, but the separation point moves backward by 25.6° compared with the separation point at *Ra* = 11 μm. This delayed flow separation and lower pressure drag result in the smallest drag coefficient at this roughness. When *Ra* > 35 μm, the drag on the legs generally tends to increase. The pressure coefficient trajectories for different surface roughnesses almost overlap, whereas the friction coefficient curves show greater variation, indicating that the drag coefficient in this roughness range is influenced primarily by friction drag. This conclusion is also supported by Fig. 21 (b), where with increasing surface roughness, the maximum friction coefficient increases, whereas the separation point position remains largely unchanged. This leads to a continuous increase in friction drag, ultimately resulting in an increase in drag on the legs.

4. CONCLUSION AND FUTURE WORK

This study investigates the impact and mechanism of ski suit surface roughness on aerodynamic performance

during the flight phase. By employing the SST–SAS turbulence model, numerical simulations are conducted for a system consisting of ski jumpers and skis. Eleven different surface roughnesses are tested at a flight speed of 29 m/s. Specifically, this study analyzes mechanical characteristics such as the lift, drag, lift–drag ratio, pitching moment, mean pressure coefficient distribution, and mean friction coefficient distribution. Additionally, flow field features obtained around the arms, trunk and legs are studied, including the mean pressure field distribution, mean velocity streamline distribution, and vortex quantity distribution. The following conclusions are drawn from the study.

The surface roughness of ski suits impacts the aerodynamic characteristics during the stable flight phase of ski jumping. Within each part of the athlete's body, the trunk generates the major contribution to the aerodynamic force. The impact of the head and neck can be neglected.

The lift–drag ratio of the entire multibody system first increases and then decreases with increasing surface roughness. It peaks at a roughness of 28 μm, with a maximum value of 1.49. From 28–48 μm, it approximately linearly decreases, stabilizing at approximately 1.44. The forward pitching moment increases almost linearly in the 8–28 μm range, peaks at 28 μm, and then linearly decreases in the 28–48 μm range. For a roughness greater than 48 μm, the pitching moment that causes the system to lean forward stabilizes at approximately 8.3 N·m.

From the perspective of achieving the optimal lift–drag ratio, a ski suit surface roughness of 28 μm offers superior aerodynamic performance, but it also results in a significant forward pitching moment. However, considering both the lift–drag ratio and pitching moment, ski suits with surface roughnesses of 8 μm and 11 μm offer commendable aerodynamic performance along with better flight stability.

Since the trunk of the ski suit contributes the most lift and drag, the surface roughness influences the aerodynamic performance by affecting the pressure drag and separation point location on the trunk, thereby significantly affecting the overall aerodynamic performance of the multibody system. The roughness of the trunk area plays an almost decisive role in the overall system's aerodynamics and should be a focal point in future ski suit development.

The impact of surface roughness on the aerodynamic performance of the arm section is manifested mainly in the backward shift of the separation point, which reduces the pressure drag on the arms. For the legs, when the surface roughness is small (Ra < 35 μm), its aerodynamic performance is influenced primarily by the position of the separation point. When the surface roughness is greater (Ra > 35 μm), the aerodynamic performance of the legs is affected mainly by frictional drag.

Future research should include wind speed as a factor to explore how surface roughness affects the aerodynamic performance of ski jumpers during the flight phase under varying wind conditions. The aerodynamic profile and angle of the skis will also be meticulously analyzed. Additionally, wind tunnel experiments with an athlete model will be conducted and compared with numerical results to further validate the reliability and universality of the findings.

ACKNOWLEDGMENTS

This work is funded by the Natural Science Foundation of Hebei Province (A2022210025) and the Central Leading Local Science and Technology Development Fund Project (236Z5410G).

CONFLICT OF INTEREST

The authors declare that they have no known competing financial interests or personal relationships that could have appeared to influence the work reported in this paper.

AUTHOR CONTRIBUTION

Kan Liu: Conceived and designed the study; wrote the manuscript; and reviewed and edited the manuscript. **Zeyuan Wang:** Conducted the experiments/data collection and analyzed the data. **Qingkuan Liu:** Provided overall supervision for the project and provided critical insights and feedback during the study design and manuscript preparation.

REFERENCES

Adams, T., Grant, C., & Watson, H. (2012). A simple algorithm to relate measured surface roughness to equivalent sand-grain roughness. *International Journal of Mechanical Engineering and Mechatronics*, *1*(2), 66-71. https://www.sci-hub.ee/10.11159/ijmem.2012.008

Cao, L., Guo, Y., Li, X., Chen, L., Wang, X., & Zhao, T. (2022). Optimization of ski attitude for the in-flight aerodynamic performance of ski jumping. *Biology*, *11*(9), 1362. https://doi.org/10.3390/biology11091362

Chowdhury, H., & Alam, F. (2014). An experimental investigation on the aerodynamic drag coefficient and surface roughness properties of sport textiles. *The Journal of the Textile Institute*, *105*(4), 414-422. https://doi.org/10.1080/00405000.2013.818757

Chowdhury, H., Moria, H., Alam, F., & Subic, A. (2011). Aerodynamics of ski jumping suits. *Sports Technology*, *4*(3-4), 164-170. https://doi.org/10.1080/19346182.2012.725411

Elfmark, O., Ettema, G., Groos, D., Ihlen, E. A., Velta, R., Haugen, P., Braaten, R., & Gilgien, M. (2021). Performance analysis in ski jumping with a differential global navigation satellite system and video-based pose estimation. *Sensors*, *21*(16), 5318. https://doi.org/10.3390/s21165318

Fritz, J., Kröll, J., Jenny, H., & Schwameder, H. (2019). In-field measurement of vertical and horizontal forces in ski-jumping: Evaluation of a portable two-dimensional force plate. *Proceedings of the*

Institution of Mechanical Engineers, Part P: Journal of sports engineering and technology, *233*(1), 126-134. https://doi.org/10.1177/1754337118809213

Gao, W., Nelias, D., Liu, Z., & Lyu, Y. (2018). Numerical investigation of flow around one finite circular cylinder with two free ends. *Ocean Engineering*, *156*, 373-380. https://doi.org/10.1016/j.oceaneng.2018.03.020

Gardan, N., Schneider, A., Polidori, G., Trenchard, H., Seigneur, J. M., Beaumont, F., Fourchet, F. & Taiar, R. (2017). Numerical investigation of the early flight phase in ski-jumping. *Journal of biomechanics*, 59, 29-34. https://doi.org/10.1016/j.jbiomech.2017.05.013

Laing, R. M., & Sleivert, G. G. (2002). Clothing, textiles, and human performance. *Textile progress*, *32*(2), 1-122. https://doi.org/10.1080/00405160208688955

Liu, K., Liu, F., & Liu, Q. (2024). Numerical investigation of an innovative windbreak design with jet flow generated by an air curtain for half-pipe skiing. *Journal of Applied Fluid Mechanics*, *17*(6), 1158-1170. https://www.sci-hub.ee/10.47176/jafm.17.6.2400

Meile, W., Reisenberger, E., Mayer, M., Schmölzer, B., Müller, W., & Brenn, G. (2006). Aerodynamics of ski jumping: experiments and CFD simulations. *Experiments in Fluids*, *41*, 949-964. https://doi.org/10.1007/s00348-006-0213-y

Moon, Y., Song, J., Kwon, K., Kwon, O., Kim, M., Yoon, S. H., Byun, Y., & A. N. Sa (2016). Development of a functional speed skating uniform through aerodynamic analysis on knit textiles and uniforms. *Journal of Engineered Fibers and Fabrics*, *11*(4), 155892501601100409. https://doi.org/10.1177/155892501601100409

Müller, W., Gröschl, W., Müller, R., & Sudi, K. (2006). Underweight in ski jumping: the solution of the problem. *International Journal of Sports Medicine*, 926-934. https://doi.org/10.1055/s-2006-923844

Nazemi, S., Khajavi, R., Far, H. R., Yazdanshenas, M. E., & Raad, M. (2018). Modeling and simulation of drag force for coated PET fabric with silica nano particles. *International Journal of Clothing Science and Technology*, *30*(3), 398-411. https://doi.org/10.1108/IJCST-09-2017-0139

Oggiano, L., Roar, S. L., Morten, B. L., & Brian, H. (2012). Air permeability and drag crisis on high tech fabrics for cross country ski competitions. *Procedia Engineering*, *34*, 15-19. https://doi.org/10.1016/j.proeng.2012.04.004

Oggiano, L., Troynikov, O., Konopov, I., Subic, A., & Alam, F. (2009). Aerodynamic behaviour of single sport jersey fabrics with different roughness and cover factors. *Sports Engineering*, *12*, 1-12. https://doi.org/10.1007/s12283-009-0029-0

Prosser, D. T., & Smith, M. J. (2016). Numerical characterization of three-dimensional bluff body shear layer behaviour. *Journal of Fluid Mechanics*, *799*, 1-26. https://doi.org/10.1017/jfm.2016.344

Pugh, L. G. C. E. (1970). Oxygen intake in track and treadmill running with observations on the effect of air resistance. *The Journal of physiology*, *207*(3), 823-835. https://doi.org/10.1113/jphysiol.1970.sp009097

Ryu, M., Cho, L., & Cho, J. (2015). Aerodynamic analysis on postures of ski jumpers during flight using computational fluid dynamics. *Transactions of the Japan Society for Aeronautical and Space Sciences*, *58*(4), 204-212. https://doi.org/10.2322/tjsass.58.204

Schwameder, H., Müller, E., Lindenhofer, E., DeMonte, G., Potthast, W., Brüggemann, P., Virmavirta, M. Isolehto, H. & Komi, P. (2005). Kinematic characteristics of the early flight phase in ski-jumping. *Science and skiing III*, 381-391. https://www.researchgate.net/publication/242339954_Kinematic_characteristics_of_the_early_flight_phase_in_ski-jumping

Seo, K., Watanabe, I., & Murakami, M. (2004). Aerodynamic force data for a V-style ski jumping flight. *Sports Engineering*, *7*, 31-39. https://doi.org/10.1007/BF02843971

Sohankar, A. (2014). A LES study of the flow interference between tandem square cylinder pairs. *Theoretical and Computational Fluid Dynamics*, *28*, 531-548. https://doi.org/10.1007/s00162-014-0329-2

Tauviqirrahman, M., Jamari, J., Wicaksono, A. A., Muchammad, M., Susilowati, S., Ngatilah, Y., & Pujiastuti, C. (2021). CFD analysis of journal bearing with a heterogeneous rough/smooth surface. *Lubricants*, *9*(9), 88. https://doi.org/10.3390/lubricants9090088

Virmavirta, M., & Kivekäs, J. (2019). Aerodynamics of an isolated ski jumping ski. *Sports Engineering*, *22*, 1-6. https://link.springer.com/article/10.1007/s12283-019-0298-1

Virmavirta, M., Isolehto, J., Komi, P., Brüggemann, G. P., Müller, E., & Schwameder, H. (2005). Characteristics of the early flight phase in the Olympic ski jumping competition. *Journal of Biomechanics*, *38*(11), 2157-2163. https://doi.org/10.1016/j.jbiomech.2004.10.004

Virmavirta, M., Kivekäs, J., & Komi, P. V. (2001). Take-off aerodynamics in ski jumping. *Journal of Biomechanics*, *34*(4), 465-470. https://doi.org/10.1016/S0021-9290(00)00218-9

Wang, Z., Liu, K., Liu, F., Wei, H., & Liu, Q. (2024). A comprehensive numerical study of the effects of surface roughness on a finite-length cylinder with an aspect ratio of 1.5 for Reynolds numbers ranging from 3.9× 103 to 4.8× 105. *Physics of Fluids*, *36*(5). https://doi.org/10.1063/5.0203141

Yamamoto, K., Tsubokura, M., Ikeda, J., Onishi, K., & Baleriola, S. (2016). Effect of posture on the aerodynamic characteristics during take-off in ski jumping. *Journal of Biomechanics*, *49*(15), 3688-

3696. https://doi.org/10.1016/j.jbiomech.2016.09.037

Zdravkovich, M. M., Brand, V. P., Mathew, G., & Weston, A. (1989). Flow past short circular cylinders with two free ends. *Journal of Fluid Mechanics*, *203*, 557-575. https://doi.org/10.1017/S002211208900159X

Zhang, L., Li, X., Wang, X., Chen, L., & Zhao, T. (2022). Performance and biomechanics in the flight period of ski jumping: Influence of ski attitude. *Biology*, *11*(5), 671. https://doi.org/10.3390/ biology11050671

Zhao Y. & Ma T., (2021, April 24-25). *Research on the application of new material technology in the field of competitive sports*. 2021 3rd International Conference on Information Science and Electronic Technology, Chongqing, China. https://doi.org/10.23977/iset2021.016